

This Page Is Inserted by IFW Operations
and is not a part of the Official Record

BEST AVAILABLE IMAGES

Defective images within this document are accurate representations of the original documents submitted by the applicant.

Defects in the images may include (but are not limited to):

- BLACK BORDERS
- TEXT CUT OFF AT TOP, BOTTOM OR SIDES
- FADED TEXT
- ILLEGIBLE TEXT
- SKEWED/SLANTED IMAGES
- COLORED PHOTOS
- BLACK OR VERY BLACK AND WHITE DARK PHOTOS
- GRAY SCALE DOCUMENTS

IMAGES ARE BEST AVAILABLE COPY.

**As rescanning documents *will not* correct images,
please do not report the images to the
Image Problems Mailbox.**

Remarks

Claims 1-5 and 15-19 have been cancelled without prejudice to prosecute them in a later application.

Examiner has rejected claims 6-15 as indefinite under 35 U.S.C. 112 because the terms "periodic structures", periodicity, amplitude and RMS are deemed vague and indefinite.

The term periodic structures is defined at page 1, lines 15-16 "The process of machining the inserts may cause periodic defects, or *periodic structures*, that may be transferred to mold halves." Thus, periodic structures are surface features on the mold insert, which are transferred onto the mold surface, and when making a silicone hydrogel, to the silicone hydrogel lens surface. See page 1, lines 22-23.

The term periodicity, amplitude and RMS are known terminology used in the art to characterize surface morphology. Periodicity is the unit repeat distance (or length) of a repeating structure measured from the front edge of a structure to the front edge of the next structure. Amplitude is height of the repeating structure. These terms are frequently used in the art as shown by "Formation and Naphthaloyl Derivatization of Aromatic Aminosilane Self-Assembled Monolayers: Characterization by Atomic Force Microscopy and Ultraviolet Spectroscopy", Langmuir, Vol., 10, No. 1 pag 149 (1994). RMS stands for "root mean square" and is calculated "by integrating the square of the height difference for the average height over the surface, dividing by the surface area and taking the square root." ^{*}"Effect of Surface Plasma Treatment on the Chemical, Physical, Morphological and Mechanical Properties of Totally Absorbable Bone Internal Fixation Devices", J. Bio. Mat. Res., vol 28, 289-301, pg 294 (1994). These are known terms used to describe surface features. Withdrawal of the rejection based upon 35 U.S.C, 112 is respectfully requested.

Claims 12 and 13 have been amended to recite that the silicone hydrogel comprises a "Group Transfer Polymerization product". Support for this amendment may be found at page 6, lines 13-15.

Applicants believe that the foregoing amendments and comments traverse the Examiner's rejections based upon 35 U.S.C. 112. Withdrawal of the 112 rejections is respectfully requested.

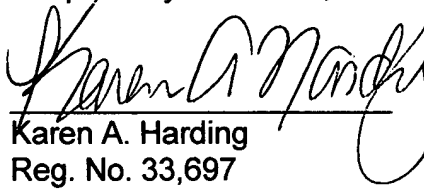
Examiner has rejected claims 6-11 as unpatentable over Nicolson (US 5,849,811). Nicolson discloses that the elastic properties (tan delta) of a polymer may be measured by compressing a disk sample in a DMA (dynamic mechanical analysis) test (See column 17, lines 15-40). As used in Nicolson the term amplitude refers to the distance that a sample of lens material is being compressed in a DMA (dynamic mechanical analysis) test.

By contrast, the term amplitude, as used in the present invention, describes the depth of imperfections on the surface of a contact lens mold. Amplitude as used in the present invention describes a mold and surface property, and is not connected with elastic properties of the lens. Thus Nicolson neither discloses nor suggests that the surface of a mold kit, mold or silicone hydrogel lens made from said mold should have periodic structures on the optically critical surface of a periodicity of less than about 3 μ m and an amplitude of less than about 4 nm RMS.

Examiner has further rejected claims 12 and 13 under 35 USC 103 as obvious over Nicolson in view of Maiden (US 6,367,929) in view of Bonafini (US 5,923,367). Neither Maiden nor Bonafini contain any disclosure regarding the size or frequency of imperfections on the surface of the mold kit, mold or silicone lenses made from said mold. Accordingly, since all three references are silent regarding the features recited in the present claims, Applicants respectfully submit that the Examiner's rejections based upon 35 USC 103 have been traversed.

Applicants respectfully submit that the rejections based upon the cited references have been overcome and should be withdrawn. A notice of allowance of all claims is respectfully submitted. If the Examiner believes that a telephone conversation would expedite the disposition of this case, the Examiner is invited to call the undersigned attorney at the telephone number listed below.

Respectfully submitted,

A handwritten signature in black ink, appearing to read "Karen A. Harding", written over a horizontal line.

Karen A. Harding
Reg. No. 33,697
Attorney for Applicants

May 16, 2003

Johnson & Johnson
One Johnson & Johnson Plaza
New Brunswick, NJ 08933-7003
(904) 443-3074

12. (Amended) The silicone hydrogel lens of claim 6, wherein the silicone hydrogel comprises a Group Transfer Polymerization product ~~Product~~ of a reaction mixture comprising 2-hydroxyethyl methacrylate, methyl methacrylate, methacryloxypropyltris(trimethylsiloxy)silane, and mono-methacryloxypropyl terminated mono-butyl terminated polydimethylsiloxane and a polymerizable mixture comprising a Si₇₋₉ monomethacryloxy terminated polydimethyl siloxane; a methacryloxypropyl tris(trimethyl siloxy) silane; N,N-dimethyl acrylamide; 2-hydroxy ethyl methacrylate; and tetraethyleneglycol dimethacrylate.

13. (Amended) The silicone hydrogel lens of claim 7, wherein the silicone hydrogel comprises a Group Transfer Polymerization product ~~Product~~ of a reaction mixture comprising 2-hydroxyethyl methacrylate, methyl methacrylate, methacryloxypropyltris(trimethylsiloxy)silane, and mono-methacryloxypropyl terminated mono-butyl terminated polydimethylsiloxane and a polymerizable mixture comprising a Si₇₋₉ monomethacryloxy terminated polydimethyl siloxane; a methacryloxypropyl tris(trimethyl siloxy) silane; N,N-dimethyl acrylamide; 2-hydroxy ethyl methacrylate; and tetraethyleneglycol dimethacrylate.

Effect of surface plasma treatment on the chemical, physical, morphological, and mechanical properties of totally absorbable bone internal fixation devices

M'hamed Ibnabddjalil,¹ Ih-Houng Loh,^{2,*} C. C. Chu,³ Norman Blumenthal,⁴ Harold Alexander,⁴ and David Turner⁵

¹Department of Theoretical and Applied Mechanics, Thurston Hall, Cornell University, Ithaca, New York 14853;

²Advance Surface Technology, Inc., Nine Linnell Circle, Billerica, Massachusetts 01821-3902; ³Department of Textiles and Apparel, Martha van Rensselaer Hall, Cornell University, Ithaca, New York 14853-4401;

⁴Department of Bioengineering, Hospitals for Joint Diseases, Orthopaedic Institute, 301 E. 17th St., New York, New York 10003; ⁵Center for Biomolecular and Materials Science Engineering, Code 6900, Naval Research Labs, Washington, DC 20375-5348

The purpose of this work was threefold: to enhance the adhesion between the reinforced absorbable calcium phosphate (CaP) fibers and the absorbable polyglycolide acid (PGA) matrix, to improve the hydrolytic degradation of the CaP fibers, and preliminarily to evaluate the cytotoxicity of the plasma treated surface of CaP fibers. A CH₄ plasma treatment was used to achieve these goals. The microbond method was used to evaluate the effects of the plasma treatment on the interfacial shear strength between the PGA matrix and CaP fibers. The treatment increased the mean interfacial shear strength of the CaP/PGA composite system by 30%. AFM data showed that CH₄-treated CaP fibers had considerable microscopic surface roughness, which facilitated mechanical interlocking between the reinforced CaP fibers and PGA matrix. The untreated and plasma-treated fibers were also subjected to *in vitro* hydrolytic degradation in a phosphate buffer solution of pH 7.44 at 37°C for up to

15 h. CH₄ plasma treatment resulted in a considerable lower polar term of the surface energy and a significantly higher disperse term in water media. This change in the proportion of surface energy terms may reduce the capillary wicking phenomena of water through the CaP fiber/PGA matrix interface. The CaP fiber dissolution studies revealed that both CH₄ and Parylene plasma polymer coatings appeared to reduce the solubility of CaP fibers, and that the magnitude of reduction was higher in an acidic than a physiologic pH environment. A preliminary cytotoxicity test revealed that both CH₄ and Parylene plasma-treated CaP fibers were noncytotoxic. Additional research should be done to determine the optimum plasma conditions and the possible use of other plasma gases to improve the interfacial shear stress of the composite and the dissolution properties of CaP fibers.

© 1994 John Wiley & Sons, Inc.

INTRODUCTION

Bioabsorbable polymers have received considerable attention for making internal fracture fixation devices. However, their mechanical properties, particularly in modulus, are not adequate for long bone fixation. To solve this problem and still preserve the benefits of biodegradability and biocompatibility of the polymer, the concept of a total bioabsorbable fiber-reinforced composite was recently introduced. The totally resorbable composite fixation plates could be classified into three main categories: 1) self-reinforced

(SR) resorbable polymeric composites in which the reinforcing material and the matrix have the same chemical composition,¹⁻⁴ 2) polymeric composites in which the matrix is chemically different from the reinforcing agent, such as a polylactide matrix reinforced with polyglycolide (PGA) fibers,⁵ and 3) semipolymeric composites in which a polymeric matrix such as poly-L-lactide (PLLA), poly-DL-lactide (PDLLA), or PGA matrix is reinforced with ceramic agents such as calcium phosphate (CaP) fibers or hydroxylapatite.⁶⁻⁸ The last category is among the most frequently studied totally bioresorbable composites. However, systems reported to date containing CaP/PLLA have generally lost substantial

*To whom correspondence should be addressed.

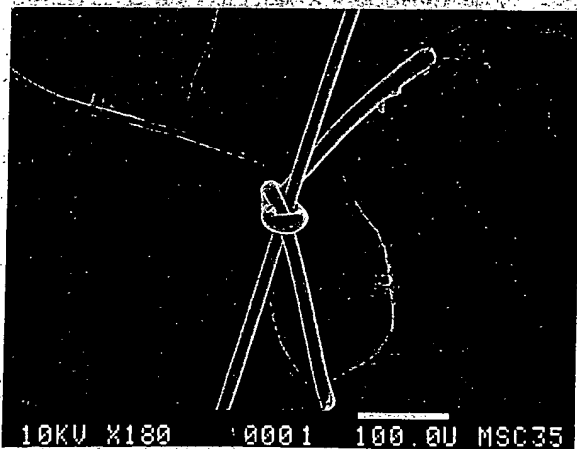


Figure 1. Knot of PGA fiber around CaP fiber with ends of the PGA fiber trimmed to about 150 μm .

strength within a few days, suggesting the ongoing difficulty of coupling such fibers with degradable polymers. These problems are: 1) the fast hydrolytic degradation of the degradable CaP fibers, 2) the weak interface between the fibers and resorbable matrices, and 3) degradation of PGA and PLLA associated with increased osteoclastic activity and osseous resorption. However, the requirements for improving the fracture toughness and increasing the hydrophobicity of the fibers seem contradictory. An improved interfacial shear strength could be achieved through either the introduction of a more hydrophobic surface (increasing the disperse component of the fiber surface energy such as the CH_4 plasma treatment reported in this article) or the incorporation of a more hydrophilic surface (increasing the polar component of the fiber surface energy)⁹ to facilitate the adhesion between the fiber and matrix.

The specific aim of this research was the use of surface modification to develop improved totally bioabsorbable fiber reinforced implants for bone fixation applications. Our study examined the use of

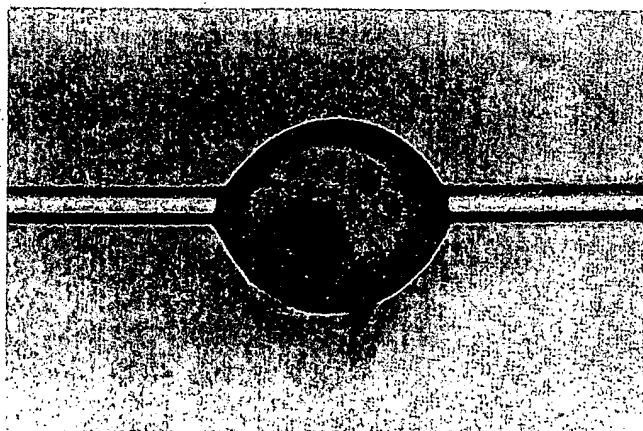


Figure 2. Optical microscopic picture of a typical microbond bead.

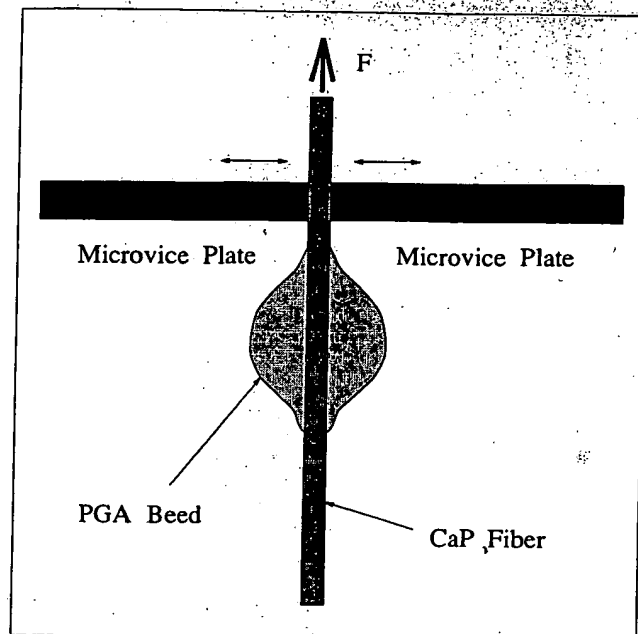


Figure 3. Schematic drawing of a microbond test.

plasma surface modification for improving the interfacial bonding between reinforced inorganic absorbable fibers and an organic matrix in totally absorbable composite bone fixation device, without the expense of the accelerated hydrolytic degradation of the reinforced fibers. The plasma surface treatment should also be expected to retard the hydrolytic degradation rate of the reinforcing fibers and their matrix, because the improved interfacial bonding would reduce the wicking of water into the interfacial space. Such an improvement offers the possibility of optimizing internal fixation of bone fractures currently encountered in totally absorbable composite materials.

MATERIALS AND METHODS

Materials

The calcium phosphate fibers used in this study were provided by Prof. LaCourse (New York State College of Ceramics, Alfred University, Alfred, NY). These fibers, with a diameter of approximately 15–20 μm , were prepared with various concentrations of CaO , ZnO , Fe_2O_3 , Na_2O , and P_2O_5 . After evaluating a large range of compositions, two types of fiber, CaP-O (23% CaO , 8% ZnO , 3% Fe_2O_3 , and 66% P_2O_5) and CaP-Na (27% CaO , 12% ZnO , 4.5% Fe_2O_3 , 2% Na_2O , and 54.5% P_2O_5), were chosen for this study.

The tensile strength of the fibers were determined on an Instron tensile testing machine using a 500 g load cell. All tensile tests were conducted at a gauge length of 20.0 mm and a crosshead speed of 1.0 mm/min.

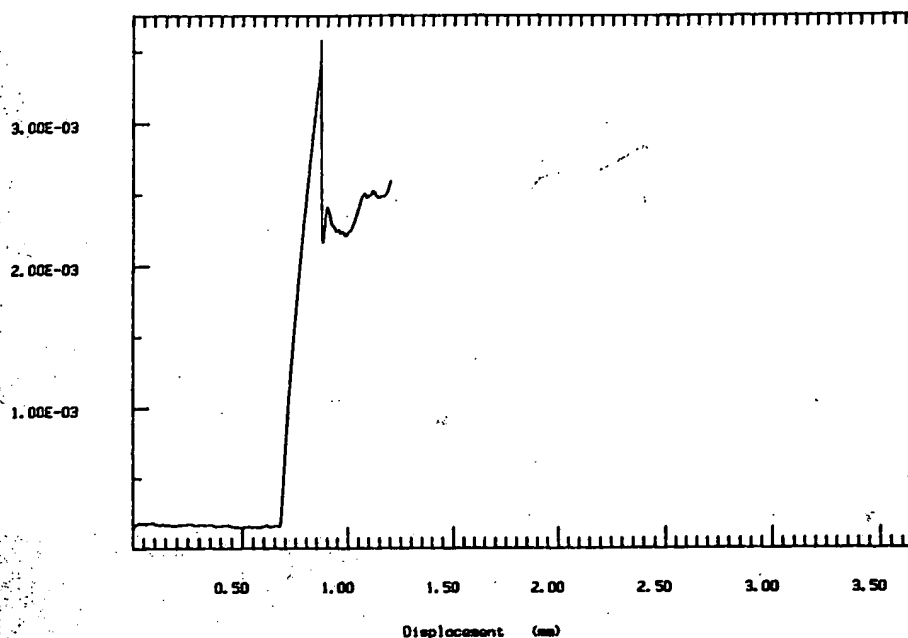


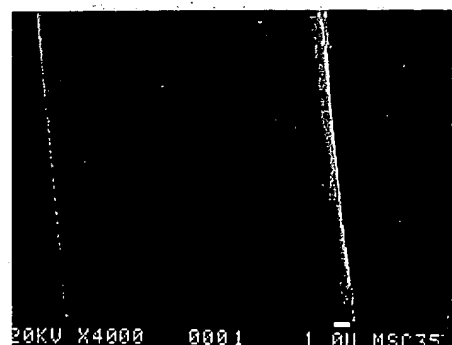
Figure 4. Typical load versus displacement plot obtained from a microbond test.

Polyglycolide acid (PGA) was used as the matrix of the composite. PGA has a melting temperature of 215°C , as determined by a Perkin-Elmer DSC with a System 4 microprocessor controller and a Model 3700 data station. The level of crystallinity was calculated to be 43.3% based on the ΔH of a theoretically 100% crystallized PGA to be 49.34 cal/g .¹⁰

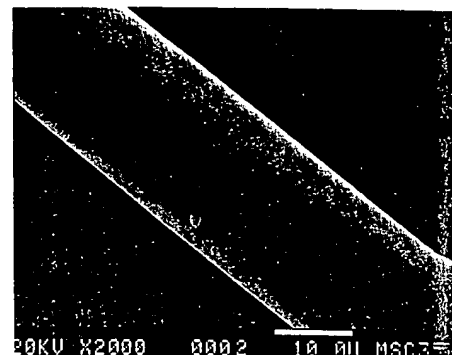
Surface plasma treatment

The surface of the calcium phosphate fibers was modified using methane (CH_4) gas plasma treatment. Some of the calcium phosphate fibers were also modified by Parylene plasma deposition for a preliminary study of their cytotoxicity and dissolution property. The details of the experiments can be found in the study by Loh et al. of synthetic absorbable suture fibers.¹¹ In brief, the experimental apparatus used for plasma surface modification consisted of a quartz reactor chamber, a radio frequency generator, a gas inlet system and controls, and a vacuum pump and control system. In a typical reaction, the specimens were mounted on a glass rack, which was then positioned in the center of the plasma chamber. The pressure of this chamber was reduced to below 0.1 mm Hg and the reacting gas monomer was introduced and allowed to flow for about 10 min before turning on the plasma. The pressure inside the reactor chamber was maintained at 50 mm Hg throughout the reaction period. The plasma was generated using a radio frequency generator operating at 13.56 MHz , and the power was controlled at the minimum required to sustain plasma, generally $50\text{--}100 \text{ W}$. The reaction proceeded for a period determined by the desired

thickness and surface energy on the substrates and the concentration of gas monomers in the reacting vapor. Typical reaction times were 10 min for the thickness (1000 \AA) required in this project. Finally, the plasma



(a)



(b)

Figure 5. Scanning electron micrographs of unhydrolyzed CaP fibers: (a) untreated fiber; (b) CH_4 plasma-treated fiber.

was turned off and inert gas (helium) gas was used to bring the vacuum system back to ambient pressure. This inert gas after treatment prevents the highly reactive radicals on the freshly treated substrate surface from causing unwanted oxidation of the surface. The reactor was returned to atmospheric pressure and the modified fibers were removed. The thickness of the plasma layer was about 1000 Å, as measured by ellipsometry. Because the thickness of the plasma layer was thin, no surface cracking or other adverse effect was observed in this and other studies.¹¹

Surface characterization

The effects of the plasma treatment were characterized by both surface wettability based on the Wilhelmy balance principle¹² and atomic force microscopy (AFM). For the surface wettability characterization, a wetting force method was used because the CaP fibers were too fine to obtain accurate and reproducible contact angles. The wetting force test was performed with a Perkin-Elmer Thermogravimetric Balance (Model TGS-2) interfaced with a Data Station (Model 3600). Three liquids (deionized water, ethylene glycol, and isopropanol) with a wide range of polarity were used in wetting force measurement. The detailed wetting force method has been described previously by Loh et al.¹¹ and Miller and Young.¹³ The work of adhesion, W_{SL} , defined as the total attraction per unit area between the two phases (fiber and liquid) can be related to contact angle by the following equation (1):

$$W_{SL}(\text{dyne/cm}) = \gamma_{LV} + \gamma_{LV} \cos \theta \quad (1)$$

where γ_{LV} is the surface tension of the liquid media. The specific wettability, w , relates to wetting force, F , as shown below:

$$w(\text{dyne/cm}) = F/\pi d \quad (2)$$

where F is the advancing wetting force (i.e., advancing weight in milligrams $\times 0.981$) recorded by a microbalance, and d is the fiber diameter (in centimeters).

All atomic force microscope images (AFM) were collected at room temperature using a Nanoscope III AFM equipped with microfabricated silicon nitride cantilevers (both from Digital Instruments, Santa Barbara, CA). The principles of standard AFM imaging have been extensively discussed elsewhere.^{14–16} CaP fiber bundles were immobilized on a flat substrate with double-stick tape, and then placed in the AFM head for imaging in air. Microfabricated silicon nitride cantilevers with tip radii of 50–100 nm and bending moduli of 0.6 N/m were used for all of the experiments. The fibers were manually positioned under the cantilever tip such that the tip was aligned over the center of a single fiber.

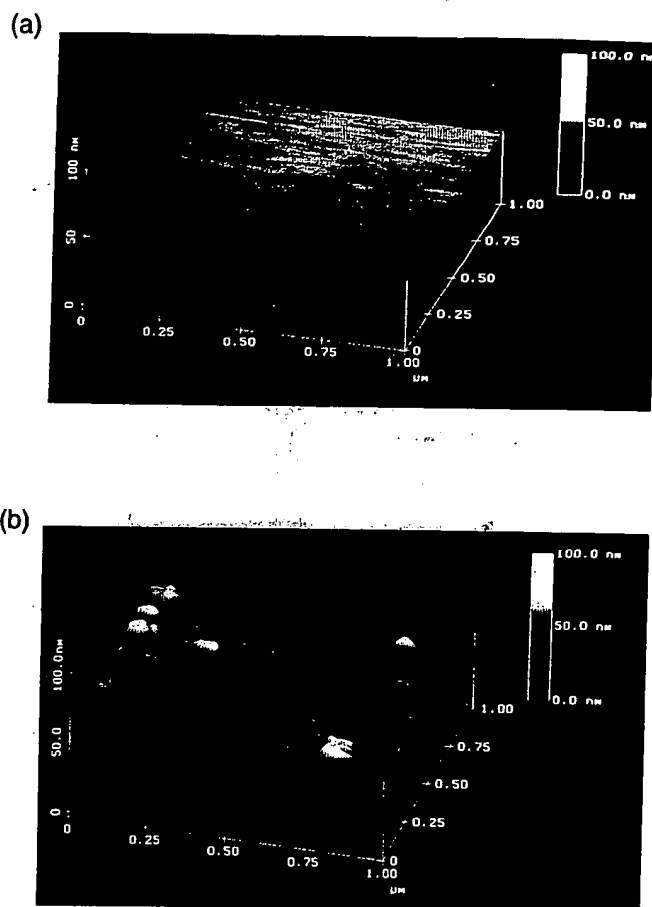


Figure 6. (a) A 1 μm AFM image of the untreated CaP control fiber. The vertical scale is a grayscale between 0–100 nm. The fiber runs from left to right across the image. The mean roughness of this surface was measured at 0.57 nm, with a maximum peak-to-peak measurement of 3.8 nm. (b) A 1 $\mu\text{m} \times 1 \mu\text{m}$ AFM image of the CH_4 -treated CaP fiber. The vertical scale is a grayscale between 0–100 nm. The fiber runs from left to right across the image. The mean roughness of this surface was measured to be 4.1 nm, with a maximum peak-to-peak measurement of 30 nm.

The Nanoscope III imaging software was then used to make the final approach of the tip to the fiber and to bring the two into contact for scanning. Images were acquired in the constant force mode with an applied force of less than 50 nN; image quality was found to be insensitive to the applied force. Digitized images were acquired over several different scan areas and then saved to computer disk for subsequent analysis.

Interfacial shear strength of CaP/PGA composite

The mechanical properties of the fiber–matrix interface have a direct impact on the strength, modulus, and toughness of the composite. This is because the surface area corresponding to the interface region can be very large (up to 3000 cm^2/cm^3 in practical composites).¹⁷

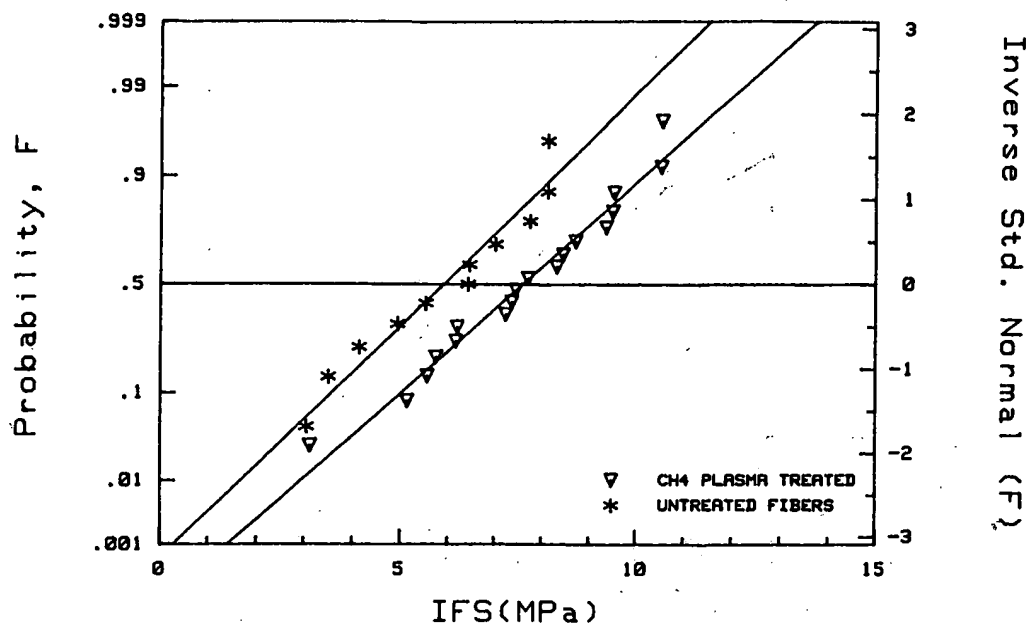


Figure 7. Interfacial shear strength results on normal probability paper: untreated fibers and CH₄ plasma-treated fibers.

that were stirred well during the solubility experiments. When aliquots were removed at each time point, the slurry that was taken out was representative of the bulk slurry due to adequate stirring. Aliquots were then centrifuged at 11,000 rpm and the clear centrifugate (0.1 mL) was analyzed by a Perkin-Elmer Model 2380 atomic absorption (AA) spectrophotometer for calcium concentration. This procedure ensured that the fiber-to-solution ratio remained unchanged over the course of each solubility experiment. For the first 60 min, a 1-mL aliquot was taken every 5 min. Subsequent aliquots were taken at 2, 3, 4, 5, and 24 h. In the calcium concentration determination by AA, 0.1 mL of the supernatant in each aliquot was placed in an atomic absorption test tube, along with 4.5 mL of LaCl₃ and 0.4 mL of deionized water. All samples were diluted in this manner to prevent the linear range of the atomic absorption spectrophotometer from being exceeded. The buffer was also analyzed for calcium, and the amount was subtracted from the value obtained for each individual sample.

Preliminary cytotoxicity study

The standard acute cytotoxicity of plasma-modified CaP fibers were examined with the assistance of the Toxikon Test Laboratory (Woburn, MA). This preliminary test was based on the USP method.²¹ The biological reactivity of a mammalian monolayer, L929 mouse fibroblast cell culture, in response to the test article was determined.

RESULTS AND DISCUSSION

Surface morphology

The surface morphologies of both untreated control and CH₄ plasma-treated CaP fibers are given in Figure 5 (SEM) and Figure 6 (AFM). SEM is suitable for examining surface features larger than 1–10 μm , whereas AFM is suitable for studying morphology at submicron length scales. SEM study revealed that both types of CaP fibers exhibited a relatively smooth surface at the given magnification. However, the AFM study revealed surface roughness of the CH₄ plasma-treated CaP fibers that were not detected by SEM. This is because AFM images were taken directly without any surface preparation, whereas SEM requires sputter coating and conductive paints, which may introduce artifacts at the submicron length scale. Figure 6(a) shows a plot of a 1 μm \times 1 μm region of the surface of the untreated fiber. The surface was smooth, with a measured RMS surface roughness of 0.57 nm and a maximum peak-to-peak variation of 3.8 nm. RMS roughness is calculated by integrating the square of the height difference from the average height over the surface, dividing by the surface area, and taking the square root. An RMS roughness of 0.57 nm is rough in comparison with a highly oriented pyrolytic graphite,¹⁵ comparable in roughness to high-quality fused silicon substrates,²² and considerably smoother than amorphous glass plates.²³ In Figure 6(b), a 1 μm \times 1 μm region of the plasma treated fiber is shown. For comparison, this was also plotted with a maximum greyscale of 100 nm. Here the surface roughness of the

TABLE III
Interfacial shear strength (IFS) in MPa of CaP Fibers/Polyglycolic Acid Matrix from Microbond Tests

	Untreated Fibers	CH ₄ Plasma-Treated Fibers
Number of specimens	11	20
Mean IFS (MPa)	5.912	7.588
Standard deviation (MPa)	1.82	1.995
Coefficient of variance (%)	32.47	26.29

treated fiber was considerably larger than that of the control fiber. The calculated RMS surface roughness for this CH₄ plasma-treated sample was 0.11 μm , with a maximum peak-to-peak variation of 0.11 μm . The roughness was also computed for several other regions on this fiber, with similar results. This microscopic surface roughness of CH₄-treated CaP increases interfacial area and hence correlates well with the increase in interfacial shear strength described subsequently.

Surface wettability

The results for the wettability test and its subsequent analysis are summarized in Tables I and II. CH₄ plasma treatment decreased the work of adhesion (W_{ad}) and the specific wettability (w). This reduction was particularly evident in water, suggesting that CH₄ plasma treatment resulted in a more hydrophobic surface on CaP fibers. These findings are consistent with the CH₄-treated synthetic absorbable sutures reported by Loh et al.¹¹ In the case of the other two less polar liquids (isopropanol and ethylene glycol), the difference between CH₄-treated and untreated controls was insignificant within the experimental errors. A detailed analysis of the wettability data based on the Harmonic-Mean Method of Wu's²⁴ revealed that the CH₄ plasma modified CaP fiber had a polar term near zero, whereas the control fiber had a polar term as high as 69.7 dyne/cm (Table II). This result

implied that the CH₄ plasma modification provided a nonpolar surface that could potentially discourage water absorption. Therefore, the ability of water to wick through the fiber-polymer interface via capillary action might be greatly reduced.

Interfacial shear strength

The mean tensile strength of untreated (16 specimens) and plasma-treated (18 specimens) CaP fibers were 375 ± 48.27 and 432 ± 51.5 MPa, respectively. The treated CaP tensile strength was not significantly higher than the strength of the untreated fibers at 95% confidence level. Because the strength of brittle fibers such as CaP is largely dictated by the presence of flaws, the number and distribution of such flaws within the fibers contribute to their typical large scatter in strength (about 10–20%). The fiber tensile strength data, therefore, should be characterized in terms of standard statistical parameters.

A typical force-displacement trace of a microbond test in which debonding occurred is given in Figure 4. The graph can be broken down into three parts: the initial friction, a linear rise up to the peak load, and then a sharp fall to some residual friction. The initial friction was intentional to make sure that the gap between the microvice plates was as close as possible, and that its magnitude was typically only a fraction of the peak load. Therefore, its effect was neglected in calculating the interfacial shear strength. Based on the assumption that the shear strength is uniform along the interface, the interfacial shear stress, τ , can be calculated from the force balance equation:

$$\tau = F_{\text{peak}}/\pi dL \quad (3)$$

where d is the diameter of the fiber and L is the length of CaP fiber embedded in the PGA matrix. The interfacial shear strength for both the untreated and plasma-treated fibers are plotted on normal probability paper, shown in Figure 7. Using the Kolmogorov-Smirnov test, the data were found to be Gaussian within a 95% confidence level. The results are summarized in Table III. The plasma-treated fibers showed a 30% increase in the mean interfacial shear strength. However, care must be taken in interpreting the results because of the inherent high variability of the microbond test. A Student t test revealed that the means for the

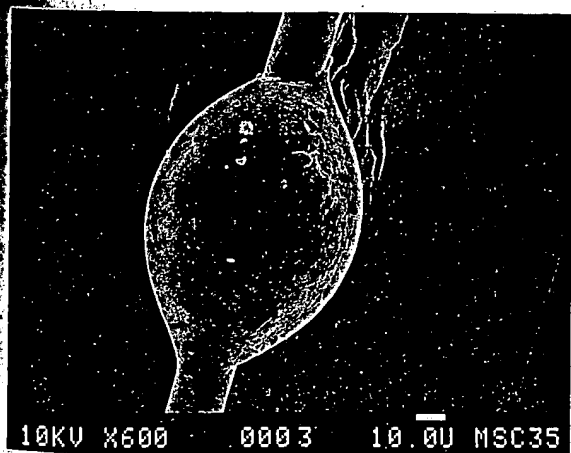


Figure 8. Scanning electron micrograph of a typical failed microbond specimen.

untreated and treated fibers were indeed different within a 95% confidence level. The observed higher IFS in the CH₄-treated CaP fiber could be partially attributed to a better mechanical interlocking between

the reinforced CaP fibers and PGA matrix, as was evident in the AFM image data previously described. SEM observations of the failed specimens showed that both the untreated and plasma-treated CaP/PGA

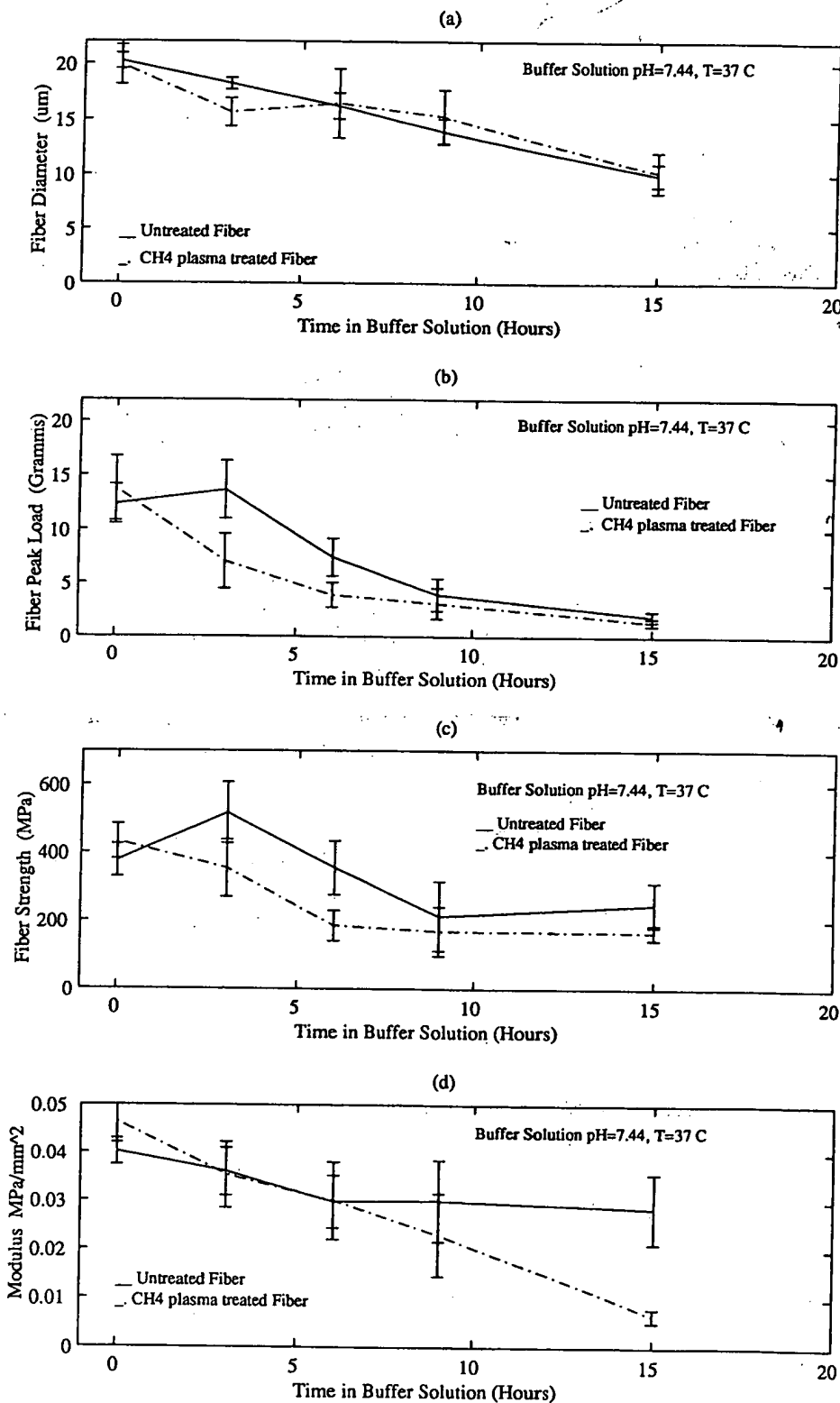


Figure 9. The changes in diameter and mechanical properties of CaP fibers in phosphate buffered solutions, pH 7.44, 37°C, for 15 h. (a) Diameter versus exposure time; (b) peak load versus exposure time; (c) tensile strength versus exposure time; (d) elastic modulus versus exposure time.

systems exhibited a clean debonding type of failure (Fig. 8).

It is important to recognize that the level of interfacial shear strength improvement also depends on the test method used to evaluate IFS. Most experimental tests evaluating the IFS fall into one of four categories: 1) the single fiber composite or fragmentation test,²⁵⁻²⁹ 2) the single fiber pullout test,³⁰⁻³² 3) the micro-indentation test,³³ and 4) the microbond test.^{18,34-36} These methods have been shown to render different IFS values. The lack of consistency among these methods does not necessarily discredit any of the methods. Their usefulness lies in determining relative changes in bond strength due to a particular surface treatment or changes in the matrix properties. The microbond method was chosen in this study for three reasons: the method is particularly suited for brittle matrices; it minimizes the adverse effects of the meniscus present in the single fiber pullout test; and only small amounts of material are needed to conduct the experiments.

In vitro hydrolytic degradation

The changes in physical and mechanical properties of CaP fibers with *in vitro* hydrolytic degradation are given in Figure 9. It seems that the degradation of the CaP fibers in buffer solution involved two stages. In the first stage, both the diameter and the strength of the fibers were affected by the buffer solution; and in the second stage, the fibers retained their strength, but the diameter reduction continued with exposure time. The untreated fibers exhibited a linear decrease in diameter with a loss of about 50% after 15 h of immersion in the buffer solution at pH 7.44. The CH₄ plasma-treated fiber had a faster loss in diameter in the first 3 h of immersion, after which the rate of degradation leveled off to that of the untreated fibers. This faster reduction in fiber diameter in the early stage of immersion corresponded to the breakdown of the plasma coating, as was evident from the SEM of the CaP fibers (Fig. 10[b]). The possible cause for this premature breakdown of the plasma layer might be the lack of chemical bonding between the CH₄ plasma layer and the CaP fibers underneath. As AFM data suggested, the improved interfacial bonding between CaP fibers and the PGA matrix was attributed to microscopic mechanical interlocking, which could be destroyed either partially or entirely by water molecules that managed to diffuse into the interfacial regions. The plasma coating was still present after the degradation rate leveled off; however, the fiber was observed to degrade at the same rate as that of the untreated fibers. For 6 h and thereafter, the diameter of the treated fibers was slightly higher than those of the untreated fibers. The difference was not significant ($P < .05$) and was therefore assumed to be the same.

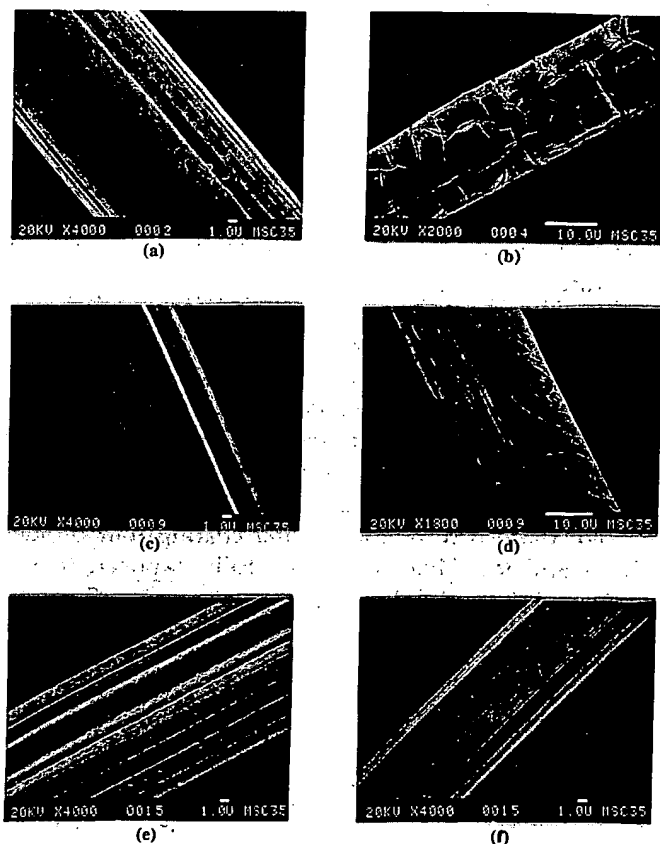


Figure 10. Scanning electron micrographs of CaP fiber after exposure to buffer solutions, pH 7.44. (a) Untreated, 3 h; (b) plasma-treated, 3 h; (c) untreated, 9 h; (d) plasma-treated, 9 h; (e) untreated, 15 h; (f) plasma-treated, 15 h.

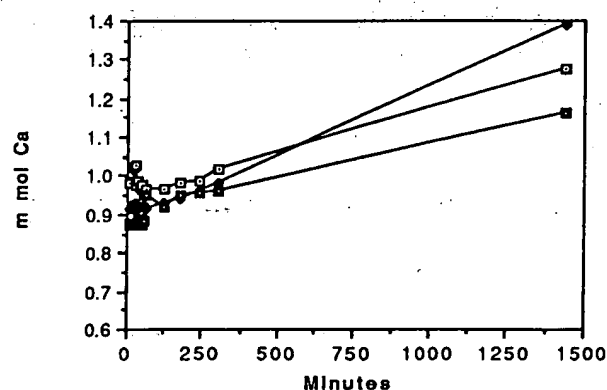
The peak load (i.e., fracture load) data were curve-fitted and exhibited a linear pattern with hydrolysis time. Both the control and plasma-treated CaP fibers showed the same linear pattern; however, the plasma-treated one had a slightly higher slope, indicating that it degraded slightly faster than the untreated control. The fiber strength of the untreated control followed a quadratic loss with hydrolysis time after an initial constant strength retention before 3 h of immersion. The CH₄-treated CaP fiber, however, exhibited the same quadratic loss of strength as the control, but over the entire immersion period (15 h) as illustrated in Figure 9(c). It is unclear why the CH₄ plasma-treated CaP fibers did not exhibit a constant strength retention during the earlier period of immersion (i.e., 3 h), as did the control. The modulus of the treated fibers decreased linearly with exposure time (Fig. 9[d]). The loss of stiffness was drastic: 80% of the original modulus was lost after 15 h of exposure time. The results for the untreated fibers showed a much slower loss of stiffness compared with those of the treated fibers. This phenomenon was similar to the previously reported study on the use of plasma treatment to overcome the adverse effect of γ irradiation of synthetic absorbable suture fibers.³⁷ The possible cause for the

faster loss of modulus of the plasma-treated CaP fibers may be attributed to the plasma skin that enveloped the CaP fibers and retarded the dissipation of acidic degradation products away from the CaP fibers. As a result, the accumulation of local acidic degradation products could lead to acid-catalyzed hydrolysis of CaP fibers. Subsequently, the CH_4 plasma-treated CaP fibers showed a faster loss in tensile strength and modulus.

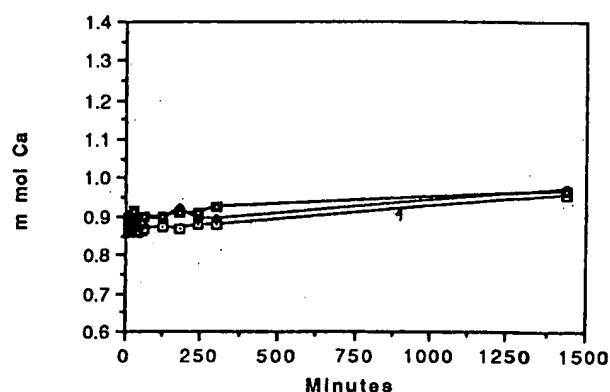
Figure 10 shows the SEM micrographs of both the untreated and treated fibers at the different stages of immersion. After 3 h in the buffer solution, the untreated fibers started to show grooves running longitudinally along the CaP fiber length. The mean fiber diameter and deeper grooves were found at a longer immersion time. The treated fibers did not exhibit the groove pattern until the plasma coating had broken down and the fibers had been fully exposed to the buffer solutions for few hours.

Dissolution of CaP fibers

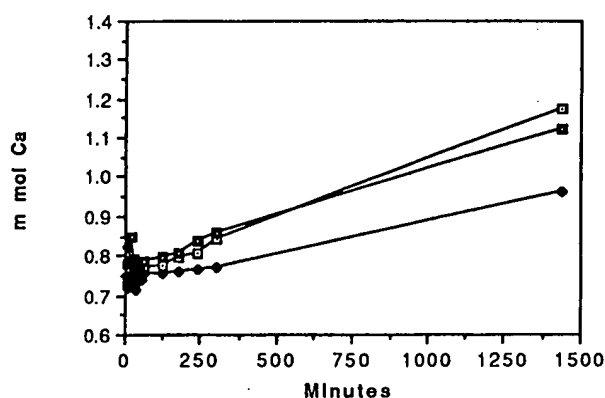
The effect of plasma treatment on the dissolution of CaP fibers (in terms of millimoles of calcium versus time, by AA spectrophotometry) in various pH media is given in Figure 11. The computed linear dissolution rates for each of the six fiber types in both buffers, after an initial dissolution burst, are shown in Table IV. The data suggest that the plasma polymer coatings appeared to affect solubility, and that the plasma-treated CaP fibers were generally less soluble than the untreated controls in both physiologic and acidic environments. CH_4 plasma had a more profound retardation on the dissolution of CaP fibers than did Parylene plasma. Within the same plasma treatment, CaP-Na fibers showed more reduction in the fiber dissolution than did CaP-O fibers. Figure 11 provides a determination of the short time dissolution kinetics of the fibers and allows a comparison of this



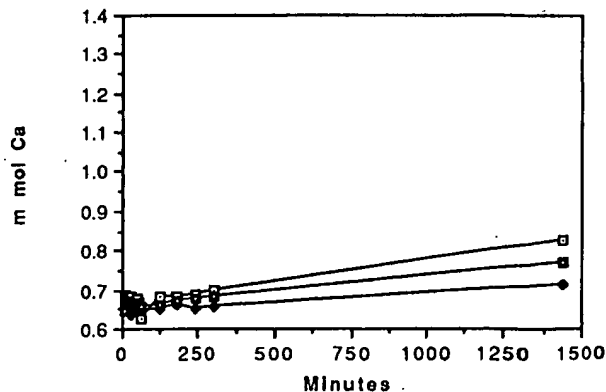
(a)



(b)



(c)



(d)

Figure 11. The effect of plasma surface treatment on the dissolution of CaP fibers in various pH media, in terms of calcium concentration (mmol) of CaP fibers measured by atomic absorption spectrophotometry as a function of time in minutes. (1) CaP-O in Tris of pH 7.4; (2) CaP-Na in Tris of pH 7.4; (3) CaP-O in acetate of pH 5.0-5.5; (4) CaP-Na in acetate of pH 5.0-5.5. \square Control; \blacktriangle CH_4 plasma; \circ Parylene plasma.

TABLE IV
Effect of Plasma Surface Treatment on CaP Fiber Dissolution Rate (mmol Ca/min $\times 10^{-4}$) in Various pH Media

	Buffer (pH)	CaP-Na Fiber	CaP-O Fiber
Control	Acetate (5.0-5.5)	1.070	2.950
CH ₄ plasma-modified	Acetate (5.0-5.5)	0.784	2.350
Parylene-modified	Acetate (5.0-5.5)	0.470	1.500
Control	Tris (7.4)	0.633	2.000
CH ₄ plasma-modified	Tris (7.4)	0.604	2.010
Parylene-modified	Tris (7.4)	0.536	3.300

TABLE V
Standard Tissue Culture Agar Overlay of Plasma Surface-Modified CaP Fibers

Sample	Biological reactivity*	Results
Positive control†	4	Severe reactivity
Negative control‡	0	Noncytotoxic
CaP-Na fibers	0	Noncytotoxic
Parylene-coated CaP fibers	0	Noncytotoxic
CH ₄ plasma-modified CaP fibers	0	Noncytotoxic
Acetone plasma-modified CaP fibers	0	Noncytotoxic

*Biological reactivity (cellular degeneration and malformation) rated on a scale from grade 0 (no reactivity) to grade 4 (severe reactivity).

†USP positive bioreaction extract/solid RS or natural rubber.

‡USP negative bioreaction RS or silicone.

process at two biologically relevant pHs. All fibers dissolved to some extent in each buffer. After 5 min, some dissolution occurred with all fibers. In fact, this initial 5 min burst accounted for over half of the calcium concentration seen after 24 h. After the initial burst, the dissolution was approximately linear with time.

The CaP-O fibers appeared to dissolve at a much higher rate than did the CaP-Na fibers in both environments. The plasma coatings seemed to retard the dissolution of the fibers; however, the effect was more consistent in the acidic (acetate) environment than it was at neutral (Tris) pH. Both CaP-O and CaP-Na fibers showed consistently decreasing dissolution rates in acetate in the following order: control, CH₄, parylene (Table IV). In Tris, the retardation of the dissolution of the CaP-O fibers was not noted. Indeed, dissolution was enhanced by the Parylene deposition.

Both sets of Parylene-coated CaP fibers appeared to be more soluble at physiologic pH than in an acidic environment, with the effect considerably more pronounced for the CaP-O fibers. The effect of pH on the hydrolytic degradation of the Parylene polymer coating remains to be elucidated. However, the apparent enhancement of dissolution above the control values for the CaP-O fibers in Tris media suggests that the deposition of the Parylene coating may alter the chemistry of the fiber surface.

The ability to change the solubility of CaP fibers in media of various pHs may be significant. This is because the glycolic or lactic acid-rich degradation

products have the potential to lower the local pH significantly in a closed space surrounded by bone. This acidity tends to cause abnormal bone resorption and/or demineralization. The resulting environment may be cytotoxic.¹⁹ Eitenmüller⁴ et al. reported that inflammatory foreign-body reactions with a discharging sinus and osteolytic foci visible on X-ray have been encountered in clinical studies.²⁰ In addition, the lowering in local pH may also result in an acid-catalyzed accelerated hydrolysis of CaP fibers.

Further research must be carried out for a more complete understanding of the dissolution behavior of the fibers. The solubility kinetics must be determined for sufficiently long periods until a steady state is reached, which is the equilibrium solubility value. Ideally, subsequent experiments should be carried out with the fibers in a separate chamber exposed to the medium, so that the risk of damage by the stirring bar is minimized. Also, the effect of serum proteins on solubility should be evaluated for a more realistic simulation of the *in vivo* situation.

Cytotoxicity

A preliminary cytotoxicity test of the fiber biocompatibility indicated that both surface modified and unmodified CaP fibers were rated to be nontoxic in cytotoxicity, as summarized in Table V.

CONCLUSIONS

The work conducted in this article has touched on several fundamental problems associated with the use of CaP/PGA composites in totally absorbable fracture plates. The weak adhesion of PGA to the CaP fibers was improved using the concept of plasma treatment. It was shown that CH₄ plasma treatment improved the interfacial shear strength of the CaP/PGA composite by 30%. This improvement can be partially attributed to a better microscopic mechanical interlocking between the plasma-treated CaP fibers and the PGA matrix. CH₄ plasma treatment also resulted in a considerably lower polar term of the surface energy and a significantly higher disperse term in water media. This change in the proportion of surface energy terms may reduce capillary wicking phenomena of water through the CaP fiber-PGA matrix interface. The plasma treatment did not affect the long-term hydrolytic degradation properties of the CaP fibers, and the *in vitro* dissolution study revealed that the plasma-treated CaP fibers were generally less soluble than was the untreated control. This effect was more pronounced in an acidic than a physiologic pH environment. Preliminary cytotoxicity study revealed that both CH₄ and Parylene plasma-treated CaP fibers were noncytotoxic. A continuation of these studies should eventually lead to a practical semiresorbable fracture fixation device.

The bulk of this study was funded by NIH-SBIR Grant 1R43-AR41086-01 to the Advanced Surface Technology, Inc. D. Turner was supported by a National Research Council postdoctoral fellowship and by the Office of Naval Research. The authors particularly thank Prof. LaCourse of Alfred University for providing CaP fibers. The technical help from Jeff Auer and the useful discussion with Prof. Anil Netravali regarding the microbond test are also acknowledged.

References

1. P. Tormala, J. Vasenius, S. Vainionpaa, J. Laiho, T. Pohjonen, and P. Rokkanen, "The ultra-high-strength absorbable self reinforced polyglycolide (sr-pga) composite rods for internal fixation of bone fractures: In vitro and in vivo study," *J. Biomed. Mater. Res.*, **25**, 1-22 (1991).
2. P. Tormala, P. Rockkanen, J. Laiho, M. Tamminmaki, and S. Vainionpaa, "Material for osteosynthesis," U.S. Patent 4,743,257 (1988).
3. P. Tormala, J. Laiho, P. Helevirta, P. Rockkanen, S. Vainionpaa, O. Bostman, and J. Kilpikari, "Resorbable surgical devices," Fifth International Conference of Polymers in Medicine and Surgery, Leeuwenhorst Congress Center, The Netherlands, 1986.
4. J. Vasenius, S. Vainionpaa, K. Vihtonen, M. Mero, J. Mikkola, P. Rockkanen, and P. Tormala, "Biodegradable self-reinforced polyglycolide (SR-PGA) composite rods coated with slowly biodegradable polymers for fracture fixation: Strength and strength retention in vitro and in vivo," *Clin. Mater.*, **4**, 307-317 (1989).
5. M. Vert, F. Chabot, J. Leray, and P. Christel, "New prosthesis parts, their preparation and their application," U.S. Patent 4,279,249 (1981).
6. M. C. Zimmerman, H. Alexander, J. R. Parsons, and P. K. Bajpai, "The design and analysis of laminated degradable composites bone plates for fracture fixation," *Hi-Tech Textiles*, T. Vigo, ed., ACS Books, Washington, D.C., 1991.
7. R. A. Casper, R. L. Dunn, and B. S. Kelly, "Totally biodegradable fracture fixation plates for use in maxillofacial surgery," Second World Congress of Biomaterials, Washington, DC, 1984, p. 278.
8. C. C. P. M. Verheyen, J. R. de Wijn, C. A. van Blitterswijk, and K. de Groot, "Evaluation of hydroxylapatite/poly(L-lactide) composites: Mechanical Behavior," *J. Biomed. Mater. Res.*, **26**, 1277-1296 (1992).
9. S. Holmes and P. Schwartz, "Amination of ultra-high strength polyethylene using ammonia plasma," *Composites Sci. Technol.*, **38**, 1-21 (1990).
10. J. Brandrup and E. H. Immergut, *Polymer Handbook*, 2nd Ed., Wiley, New York, 1975, p. 33.
11. I. H. Loh, H. L. Lin, and C. C. Chu, "Plasma surface modification of synthetic absorbable sutures," *J. Appl. Biomater.*, **3**, 131-146 (1992).
12. J. Wilhelmmy, "Annalen Der Physik und Chemie," *Annalen der Physik*, **119**, 177 (1863).
13. B. Miller and R. A. Young, "Methodology for studying the wettability of filaments," *Textile Research Journal*, **45**, 359-365 (1975).
14. G. Binnig, C. F. Quate, and C. Gerber, "Atomic force microscopy," *Phys. Rev. Lett.*, **56**, 930 (1986).
15. G. Binnig, C. Gerber, E. Stoll, T. R. Albrecht, and C. F. Quate, "Atomic resolution with atomic force microscope," *Europhys. Lett.*, **3**, 1281 (1987).
16. D. Ruger and P. Hansma, "Atomic force microscopy," *Physics Today*, October, 23 (1990).
17. K. K. Chawla, *Composite Materials: Science and Engineering*, Springer Verlag, New York, 1987.
18. K. P. McAlea and G. J. Besio, "Adhesion between polybutylene terephthalate and e-glass measured with the microbond technique," *Polymer Composites*, **9**, 285-290 (1988).
19. A. U. Daniels, M. S. Taylor, K. P. Andriano, and J. Heller, "Toxicity of absorbable polymers proposed for fracture fixation devices," *Trans. 38th Ann. Mtg. Orthop. Res. Soc.*, **17**, 88 (1992).
20. J. Eitenmüller, K. L. Gerlach, T. Schmickal, and G. Muhr, "Die Versorgung von Springelenksfrakturen unter Verwendung von Platten und Schrauben aus resorbierbarem Polymer material," presented at Jahrestagung der Deutschen Gesellschaft für Unfallheilkunde, Berlin, November 1989.
21. USP XXII, pp. 1495-1496, 1990, and Supplement 5, pp. 2702-2703, 1991.
22. D. Turner and D. Stenger, unpublished observations.
23. J. P. K. Peltonen, H. Pingsheng, and J. B. Rosenholm, "Order and defects of Langmuir-Blodgett films detected with the atomic force microscope," *J. Am. Chem. Soc.*, **114**, 7637 (1992).
24. S. Wu, "Surface tension and polarity of solid polymers," in *Polymer Interface and Adhesion*, S. Wu, ed., Chapter 5, Marcel Dekker, New York, 1982.
25. L. T. Drzal, M. J. Rich, and P. F. Lloyd, "Adhesion of graphite fibres to epoxy matrices: I. The role of fiber surface treatment," *J. Adhesion*, **16**, 1-30 (1982).

16. E. T. Drzal, M. J. Rich, M. F. Koenig, and P. F. Lloyd, Adhesion of graphite fibres to epoxy matrices: II. The effect of fiber finish," *J. Adhesion*, **17**, 133-152 (1983).
17. S. H. Own, "A statistical theory of interfacial shear strength distribution and its application to carbon-fiber reinforced polymer composites," PhD thesis, Washington State University, Pullman, 1984.
18. S. H. Own, R. V. Subramanian, and S. C. Sanders, "Bimodal lognormal model of the distribution of strength of carbon fibers: Effects of electrodeposition of titanium di(dioctyl pyrophosphate) oxyacetate," *J. Mater. Sci.*, **21**, 3912-3920 (1986).
19. A. N. Netravali, R. B. Henstenburg, S. L. Phoenix, and P. Schwartz, "Interfacial shear strength studies using the single filament composite test. I. Experiments on graphite fibers in epoxy," *Polymer Compos.*, **10**, 226 (1989).
20. P. S. Chua and M. R. Piggott, "The glass fiber-polymer interface: I. Theoretical consideration for single filament pullout test," *Compos. Sci. Tech.*, **22**, 33-42 (1985).
21. J. P. Favre and M. C. Merienne, "Characterization of fiber/resin bonding in composites using a pull out test," *Int. J. Adhesion Adhesives*, **1**, 311-316 (1981).
22. L. S. Penn and S. M. Lee, "Interpretation of the force trace for kevlar/epoxy single filament pullouts tests," *Fibre Science and Technology*, **17**, 91-97 (1982).
23. D. B. Marshall and W. C. Oliver, "Measurement of the interfacial mechanical properties in fiber-reinforced ceramic composites," *J. Am. Ceram. Soc.*, **70**, 542-548 (1987).
24. B. Miller, P. Muri, and L. Rebenfeld, "A microbond method for the determination of the shear strength of fiber/resin interface," *Comp. Sci. Tech.*, **28**, 17-32 (1987).
25. R. A. Haaksma and M. J. Cehelnik, "A critical evaluation of the use of the microbond method for the determination of composite interfacial properties," *Material Research Society Symposia Proceedings*, 1990, pp. 71-76.
26. U. Gaur, G. Desio, and B. Miller, "Measuring fiber/matrix adhesion in thermoplastic composites," *Plastic Engineering*, October, 43-45, (1989).
27. L. Zhang, C. C. Chu, and I.-H. Loh, "Effect of combined gamma irradiation and parylene plasma treatment on the hydrolytic degradation of synthetic biodegradable sutures," *J. Biomed. Mater. Res.*, **27**, 1425-1441 (1993).

Received April 28, 1993

Accepted September 5, 1993

Formation and Naphthoyl Derivatization of Aromatic Aminosilane Self-Assembled Monolayers: Characterization by Atomic Force Microscopy and Ultraviolet Spectroscopy

Charles N. Durfor,*† David C. Turner,‡ Jacque H. Georger,\$|| Brian M. Peek,† and David A. Stenger*‡

Center for Bio/Molecular Science and Engineering, Code 6900, Naval Research Laboratory, Washington, D.C. 20375-5348, HFM-594, CBER, Food and Drug Administration, 8800 Rockville Pike, Bethesda, Maryland 20892, and Geo-Centers, Inc., Ft. Washington, Maryland 20744

Received March 25, 1993. In Final Form: July 23, 1993*

Self-assembled monolayers (SAMs) prepared from short chain aminoalkyl- and aromatic aminoalkylsilanes have recently proven valuable in controlling the adhesive properties of silica substrates for chemical, biological, and microelectronic applications. To gain insight to the structure and amine reactivity of these films, we have studied the formation of SAMs formed on silica surfaces from (((aminoethyl)amino)methyl)phenethyl)trimethoxysilane (PEDA), and their modification with 2-naphthoyl chloride (NAP-Cl). Atomic force microscopy was used to demonstrate that PEDA and PEDA-NAP SAMs do not pack in a periodic or regular array on the surface but in fact are highly disordered relative to surface-deposited Langmuir-Blodgett (LB) phospholipid films, organothiol SAMs on gold, and at least one perfluorinated alkyl monochlorosilane SAM. In contrast to chromophores in well-ordered monolayers, the UV absorbance lineshapes and ratio of peaks corresponding to the $^1A \rightarrow ^1B_u$ and $^1A \rightarrow ^1L_a$ transitions of the NAP chromophore remain relatively unchanged after immobilization. A simple first-order model, used to estimate molecular densities and reaction stoichiometries, suggests that in reaction-site-limited PEDA SAMs, the amine reactivity is limited by the maximum packing density of the NAP chromophore.

Introduction

Self-assembled monolayers (SAMs)^{1,2} prepared from short chain (<10 carbons) aminoalkyl- and aromatic aminoalkylsilanes have proven valuable for surface modification in electrochemistry³ and more recently for molecular patterning in microelectronics,⁴ surface grafting reactions,⁵ and cell biology.⁶⁻⁸ These applications rely on the ability of surface amine groups to complex or react covalently with solution phase molecules. However, unlike SAMs prepared from organothiols on gold,^{9,10} carboxylic acids on alumina,¹¹ or surface layers prepared by Langmuir-Blodgett (LB) deposition,¹²⁻¹⁸ very little information exists on the relationship between the structure and

properties of aminosilane films. A putatively high degree of disorder in these films,^{8,19} which has not been experimentally confirmed, has complicated the interpretation of results obtained using conventional techniques such as ellipsometry and wettability. Furthermore, the chemical properties of these films, such as those relating to amine accessibility and reactivity, require further investigation.

In this paper, we report on the formation and structural properties of SAMs prepared from (((aminoethyl)amino)methyl)phenethyl)trimethoxysilane (PEDA) and their modification with 2-naphthoyl chloride (NAP-Cl). Chemical structures for both are shown in Figure 1. Structurally, we have characterized these films using ellipsometry, wettability, and atomic force microscopy (AFM) to determine the thickness and intermolecular packing order of the SAMs. Atomic force microscopy (AFM) has become a standard tool for determining the two-dimensional structural packing order of organothiol SAMs on gold⁹ and Langmuir-Blodgett films.^{12,13,16-18,20} Recently, Mathauer and Frank²¹ have shown that SAMs formed from (11-(2-naphthyl)undecyl)trichlorosilane and octadecyltrichlo-

* Food and Drug Administration.

† Naval Research Laboratory.

‡ Geo-Centers, Inc.

|| Current address: Shipley Company, Inc., Marlborough, MA 01752.

* Abstract published in *Advance ACS Abstracts*, December 1, 1993.

(1) Swalen, J. D.; Allara, D. L.; Andrade, J. D.; Chandross, E. A.; Garoff, S.; Israelachvili, J.; McCarthy, T. J.; Murray, R.; Pease, R. F.; Rabolt, J. F.; Wynne, K. J.; Yu, H. *Langmuir* 1987, 3, 932-950.

(2) Ulman, A. *Introduction to Ultrathin Organic Films*; Academic Press, Inc.: San Diego, CA, 1991, and references contained therein.

(3) Moses, P. R.; Wier, L. M.; Lennox, J. C.; Finklea, H. O.; Lenhard, J. R.; Murray, R. W. *Anal. Chem.* 1978, 50, 576-585.

(4) Calvert, J. M.; Chen, M. S.; Dulcey, C. S.; Georger, J. H.; Peckerar, M. C.; Schnur, J. M.; Schoen, P. E. *J. Vac. Sci. Technol. B* 1991, 9, 3447-3450.

(5) Massia, S. P.; Hubbell, J. A. *J. Biomed. Mater. Res.* 1991, 25, 223-42.

(6) Dulcey, C. S.; Georger, J. H.; Krauthamer, V.; Stenger, D. A.; Fare, T. L.; Calvert, J. M. *Science* 1991, 252, 551-554.

(7) Kleinfeld, D.; Kahler, K. H.; Hockberger, P. E. *J. Neurosci.* 1988, 8, 4098-4120.

(8) Stenger, D. A.; Georger, J. H.; Dulcey, C. S.; Hickman, J. J.; Rudolph, A. S.; Nielsen, T. B.; McCort, S. M.; Calvert, J. M. *J. Am. Chem. Soc.* 1992, 114, 8435-8442.

(9) Alves, C. A.; Smith, E. L.; Porter, M. D. *J. Am. Chem. Soc.* 1992, 114, 1222-1227.

(10) Nuzzo, R. G.; Dubois, L. H.; Allara, D. L. *J. Am. Chem. Soc.* 1990, 112, 558-69.

(11) Chen, S. H.; Frank, C. W. *Langmuir* 1991, 7, 1719-1726.

(12) Peltonen, J. P. K.; Pingsheng, H.; Rosenholm, J. B. *J. Am. Chem. Soc.* 1992, 114, 7637-7642.

(13) Goettgens, B. M.; Tillmann, R. W.; Radmacher, M.; Gaub, H. E. *Langmuir* 1992, 8, 1768-1774.

(14) Durfee, W. S.; Storck, W.; Willig, F.; von Frieling, M. *J. Am. Chem. Soc.* 1987, 109, 1297-1301.

(15) Saito, K.; Ikegami, K.; Kuroda, S. I.; Saito, M.; Tabe, Y.; Sugi, M. *J. Appl. Phys.* 1990, 68, 1968-1974.

(16) Weisenhorn, A. L.; Drake, B.; Prater, C. B.; Gould, S. A. C.; Hansma, P. K.; Ohnesore, F.; Egger, B. M.; Heyn, S. P.; Gaub, H. E. *Biophys. J.* 1990, 58, 1251-1258.

(17) Egger, B. M.; Ohnesore, F.; Weisenhorn, A. L.; Heyn, S. P.; Drake, B.; Prater, C. B.; Gould, S. A. C.; Hansma, P. K.; Gaub, H. E. *J. Struct. Biol.* 1990, 103, 89-94.

(18) Zasadzinski, J. A. N.; Helm, C. A.; Longo, M. L.; Weisenhorn, A. L.; Gould, S. A. C.; Hansma, P. K. *Biophys. J.* 1991, 59, 755-760.

(19) Stenger, D. A.; Pike, C. J.; Hickman, J. J.; Cotman, C. W. *Brain Res.*, in press.

(20) Marti, O.; Ribi, H. O.; Drake, B.; Albrecht, T. R.; Quate, C. F.; Hansma, P. K. *Science* 1988, 239, 50-52.

(21) Mathauer, K.; Frank, C. Submitted to *Langmuir*.

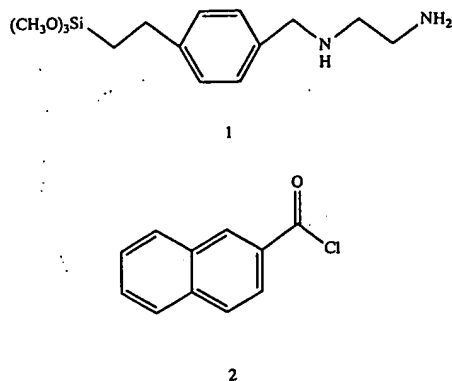


Figure 1. The molecular structure of *p,m*-(((aminoethyl)amino)methyl)phenethyl)trimethoxysilane or PEDA (1) and 2-naphthoyl chloride or NAP-Cl (2).

rosilane exhibit large changes in the absorbance ratio of the ${}^1\text{A} \rightarrow {}^1\text{B}_u$ and ${}^1\text{A} \rightarrow {}^1\text{L}_a$ transitions of naphthalene upon immobilization into well-ordered SAMs. Thus, we have also compared the UV spectra of PEDA and NAP-PEDA in solution and on surfaces to gain information on possible molecular orientations.

The spectroscopic data described in this paper suggest that electronic changes for the PEDA and NAP-PEDA chromophores are minimal upon surface immobilization and correlate with a high degree of disorder observed by AFM. First-order calculation of PEDA and NAP-PEDA SAM packing densities from the spectra are in qualitative agreement with previous analyses of surface silanol densities,²² the molecular densities of aromatic silanes as determined by X-ray diffraction,²³ and the packing density of naphthalene crystals.²¹ Measured ratios of NAP-PEDA to PEDA absorbances, showing the relationship between the amine reactivity and PEDA surface density, suggest that the reaction is limited by the maximum surface packing density of the NAP chromophore.

Materials and Methods

Reagents. (((Aminoethyl)amino)methyl)phenethyl)trimethoxysilane (PEDA) was obtained from Hüls America, Inc. (Piscataway, NJ), and 2-naphthoyl chloride (NAP-Cl) from Aldrich Chemical Co. (Milwaukee, WI). Other reagents were obtained in the highest commercial purity and used as received. Solution reaction of NAP-Cl was performed in Burdick and Jackson acetonitrile (Baxter Healthcare Corp., Muskegon, MI).

Surface Modification. All liquid and surface chemistries were performed under a helium atmosphere in a drybox (Vacuum Atmospheres Model HE-43-2, Hawthorne, CA). Substrate preparation and modification were performed as previously described.^{6,8} Fused silica slides (1 in. \times 1 in.), Dell Optics, Fairview, NJ) and polished native Si (100) wafers (WaferNet, Inc., San Jose, CA) were reacted with acetonitrile containing 1.0 mM acetic acid, 5% deionized water, and 0.33–330 mM (i.e., 0.1–10% (v/v)) PEDA. All reactions were conducted at room temperature and film formation times were varied from 3 min to 24 h. Following the reaction, the substrates were washed 3 times with acetonitrile and heat cured on a temperature-controlled hot plate set at 120 °C for 3 min prior to spectral analysis. NAP-PEDA films were prepared by reacting PEDA SAMs in a solution of 1% (w/v) NAP-Cl in anhydrous acetonitrile for 1 h. Reaction byproducts were removed by four acetonitrile washes. Ellipsometry and atomic force microscopy studies of PEDA films were correlated with UV spectroscopic analyses by preparing silanized silicon wafers and fused silica slides in the same reaction solution.

Optical Ellipsometry and Wettability Measurements. Thickness measurements of SAMs on Si wafers were performed with a Gaertner Model 115C ellipsometer (Chicago, IL) equipped with a helium–neon laser (632.8 nm), using a 70° angle of incidence and a compensator setting of -45° . Optical constants of the individual substrate wafers were determined prior to silanization by treating the bulk Si and oxide collectively as a single material.^{23,24} Film thicknesses were then determined at nine points on each silanized wafer using the substrate optical constants and the manufacturer-listed bulk refractive index of 1.508 for PEDA. The advancing water contact angles were measured for each substrate type as previously described⁸ using an NRL Zisman type goniometer by application of static, sessile drops (5–30 μL) of deionized water to the substrate surfaces with a micropipetter.

Atomic Force Microscopy. All atomic force microscope (AFM) images were collected at room temperature (approximately 22 °C) using a Nanoscope III AFM equipped with microfabricated silicon nitride cantilevers (both from Digital Instruments, Santa Barbara, CA). Samples were immersed in deionized water and then imaged using the fluid cell attachment for the AFM. All images were acquired as raster scans in a constant force mode with a force of less than 10 nN. Polished native oxide silicon wafers were used as supports for the silanes rather than fused silica slides because the root mean square surface roughness is less than 0.1 nm over a 1 μm region, allowing for high resolution imaging with the AFM. Sequential scans were reproducible and remained consistent when the scanning direction was rotated by 30°. Images were filtered by applying a two-dimensional fast Fourier transform, removing weak high frequency points, and then applying a reverse transform.

Ultraviolet Spectroscopy. All solution and solid phase UV spectra were determined with a Cary 2400 (UV-VIS-NIR) spectrophotometer (Varian, Sugarland, TX). Solution spectra were measured in gas-tight cuvettes under a helium atmosphere. Absorbance measurements are given in terms of absorbance units (au) at a particular wavelength. The following equation was used to calculate absorbance

$$\text{absorbance} = A = \log_{10}(I_0/I_t) \quad (1)$$

where I_0 is the incoming intensity and I_t is the outgoing intensity after passing through the sample.²⁵ Values of the molar extinction coefficient, ϵ_{molar} , were determined by measuring the UV spectra of known concentrations of PEDA, NAP-Cl, or NAP-PEDA in acetonitrile.

Results

Atomic Force Microscopy. The physical structures of PEDA and NAP-PEDA surfaces were examined by atomic force microscopy (AFM) and compared to periodically ordered films. Typical AFM images of well-ordered, condensed Langmuir–Blodgett films transferred to flat substrates show periodic corrugations about 0.1–0.2 nm in height with row spacings of 0.5–0.8 nm.^{16–18,26} The tight packing of the lipid hydrocarbon films in these samples reduces the size of the height variations by not allowing the AFM tip to penetrate into the film. Thus, the periodic corrugations reflect the ordered packing of molecules in the film. We have recently observed the same periodic row structure in SAMs prepared from (tridecafluoro-1,1,2,2-tetrahydrooctyl)dimethylchlorosilane (13F), as shown in Figure 2a.²⁶ Corrugations are observed with a periodicity of 0.5 nm and amplitude of 0.15 nm, in good agreement with what is expected of a uniform surface of close-packed fluorocarbon chains.

(24) Azzam, R. M. A.; Bashara, N. M. *Ellipsometry and Polarized Light*; North Holland Publishing Company: Amsterdam, 1977.

(25) Silverstein, R. M.; Bassler, G. C.; Morrill, T. C. *Spectrometric Identification of Organic Compounds*, 4th ed.; John Wiley & Sons: New York, 1981.

(26) Fare, T. L.; Palmer, C. A.; Silvestre, C. G.; Cribbs, D. H.; Turner, D. C.; Brandow, S. L.; Gaber, B. P. *Langmuir* 1992, 8, 3116–3121.

(22) Gun, J.; Iscovic, R.; Sagiv, J. *J. Colloid Interface Sci.* 1984, 101, 201–213.

(23) Wasserman, S. R.; Whitesides, G. M.; Tidswell, I. M.; Ocko, B. M.; Pershan, P. S.; Axe, J. D. *J. Am. Chem. Soc.* 1989, 111, 5852–5861.

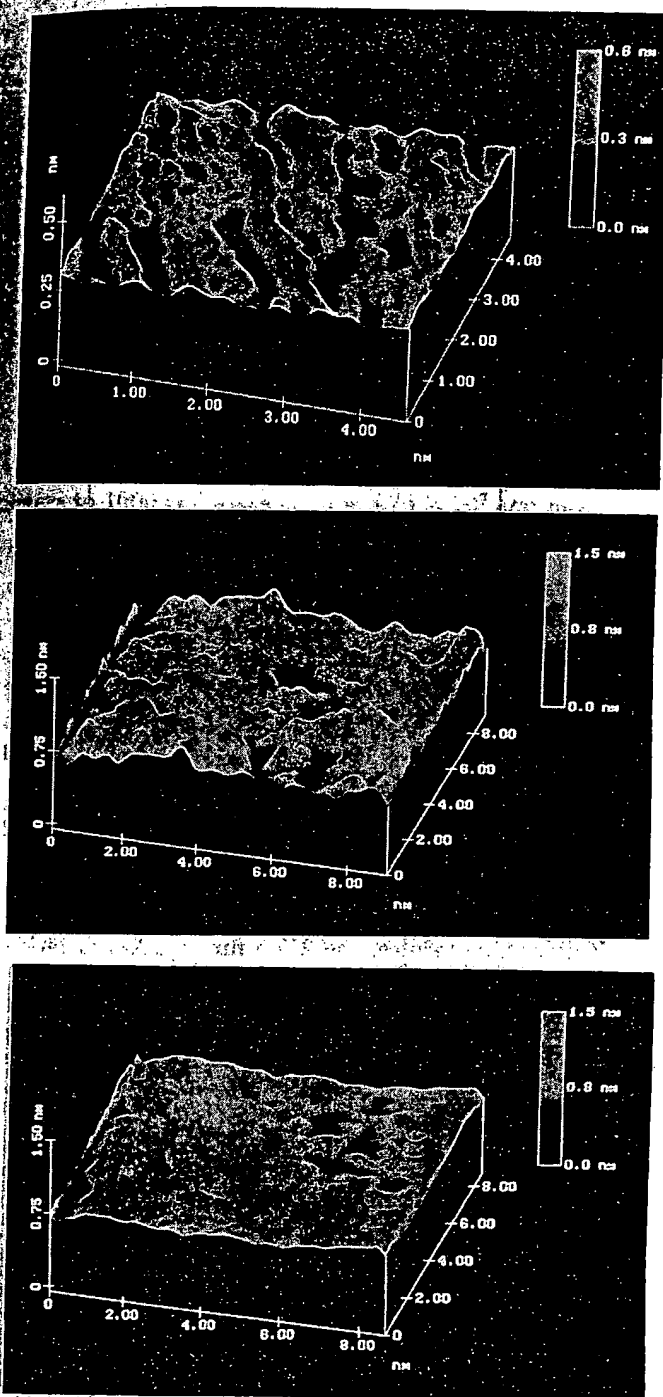


Figure 2. AFM images of SAMs formed on the native oxide of polished Si wafers. (a, top) A 0.46 by 0.46 nm AFM image of a 13F SAM (image courtesy of Dr. Susan Brandow). The gray scale indicates the height of the surface as indicated by the bar on the right-hand side of the image. (b, middle) A 0.9 by 0.9 nm image of a PEDA SAM. Note that the height scale is now 1.5 nm, 3 times larger than the scale for 13F. The PEDA surface shows no signs of the periodic structure indicative of an ordered film and is characterized by a peak-to-peak surface roughness of 0.5 nm. (c, bottom) A 0.9 by 0.9 nm image of a NAP-derivatized PEDA SAM. This surface has a peak-to-peak roughness of 0.3 nm and is consistent with a disordered packing of the molecules on the film.

AFM gray-scale images of reaction-site-limited PEDA and NAP-PEDA SAMs are shown in parts b and c of Figure 2, respectively. The images cover a representative 9 × 9 nm region of the surface with a maximum scale in the vertical direction of 1.5 nm, which is 3 times larger than the vertical scale in the 13F image in Figure 2a. In sharp contrast to the corrugations of the 13F surface, these

Table 1. Spectral Properties of Naphthalene Derivatives^a

compound	λ_{\max} (nm)	ϵ_{molar} (M ⁻¹ cm)
2-naphthoyl acid chloride	249.5	48 000
2-naphthoyl acid	236.5	52 700
2-naphthoyl acid anion	229.5	55 230
2-naphthoyl-PEDA conjugate	226.5	53 800

^a Solution phase λ_{\max} and ϵ_{molar} for NAP-Cl and its reaction products. 20 mM NAP-Cl and NAP-PEDA solutions were prepared as discussed in the Materials and Methods section. 20 mM solutions of naphthoyl acid and naphthoyl acid anion were prepared in 1.0 M HCl and 50 mM pH 9.0 borate buffer, respectively. The ϵ_{molar} for the 2-naphthoyl-PEDA conjugate (NAP-PEDA) represents the difference in NAP-PEDA and PEDA solution absorbances.

films show no evidence of a periodic regular structure. The PEDA surface is much rougher than the 13F surface with a vertical peak-to-peak variation of 0.5 nm within the 9 × 9 nm region. This variation is nearly 50% of the mean thickness of 12 ± 2 Å that was determined by ellipsometry. The peak-to-peak surface roughness of the NAP-PEDA SAM is somewhat less, 0.3 nm, but still twice as large as that measured for the tightly packed monolayer of 13F. This may be due to the NAP-Cl filling some of the "holes" observed in the PEDA SAM. Nonetheless, both images are consistent with a random arrangement of the molecules on the surface that is disordered with respect to both position and orientation and contains abundant defects.

UV Absorbance of PEDA and NAP-PEDA SAMs. NAP-Cl was chosen as a suitable PEDA SAM labeling reagent for a variety of reasons. First, naphthalene is a sensitive optical probe having ¹A⁻B_b and ¹A⁻L_a dipole transition moments that are parallel to the long and short axes, respectively, of the molecule.²⁷ This makes naphthyl derivatives highly useful for the study of molecular orientation effects in polymers²⁸ and SAMs.²¹ Second, naphthalene is smaller than many chromophores (e.g., fluorescein or porphyrins), permitting higher surface packing densities. Third, NAP-Cl and its reaction products with water and amines are well-resolved spectrally (Table 1). Finally, naphthoyl chloride reacts quickly with amino groups in the PEDA SAM to form amide bonds. The only possible side product would result from reaction with silanol groups at the surface or in the film. However, the ester formed would be unstable to hydrolysis or reaction with amines and would not be expected to significantly affect the UV properties of the film.

The UV solution spectra of PEDA, NAP-PEDA, and NAP-Cl in acetonitrile are shown in Figure 3a. The UV spectra of PEDA and NAP-PEDA SAMs on fused silica are shown in Figure 3b. The acetonitrile solution spectra of PEDA exhibit a λ_{\max} at 193 nm, while PEDA SAMs on fused silica have a λ_{\max} of 195 nm. Significantly, both spectra have similar line shapes. In order to directly compare the NAP UV spectrum in solution with the NAP UV spectrum of the SAM, the solution spectrum of PEDA was subtracted from an equimolar NAP-PEDA solution, and the spectrum of a PEDA SAM was subtracted from its corresponding NAP-PEDA SAM. The resulting spectra are those of the NAP amide after reaction with an amine of PEDA in solution or in a PEDA SAM. The NAP-PEDA difference solution spectrum had $\lambda_{\max} = 226.5$ nm, and the NAP-PEDA SAM difference spectrum had $\lambda_{\max} = 227.5$ nm. As in the PEDA SAMs, both of the NAP difference spectra had similar line shapes. The red-shifts of 2 and 1 nm for PEDA and NAP-PEDA following immobilization are consistent solvatochromic effects re-

(27) Kleven, H. B.; Platt, J. R. *J. Chem. Phys.* 1949, 17, 470-481.

(28) Semerak, S. N.; Frank, C. W. *Adv. Polym. Sci.* 1983, 54, 31.

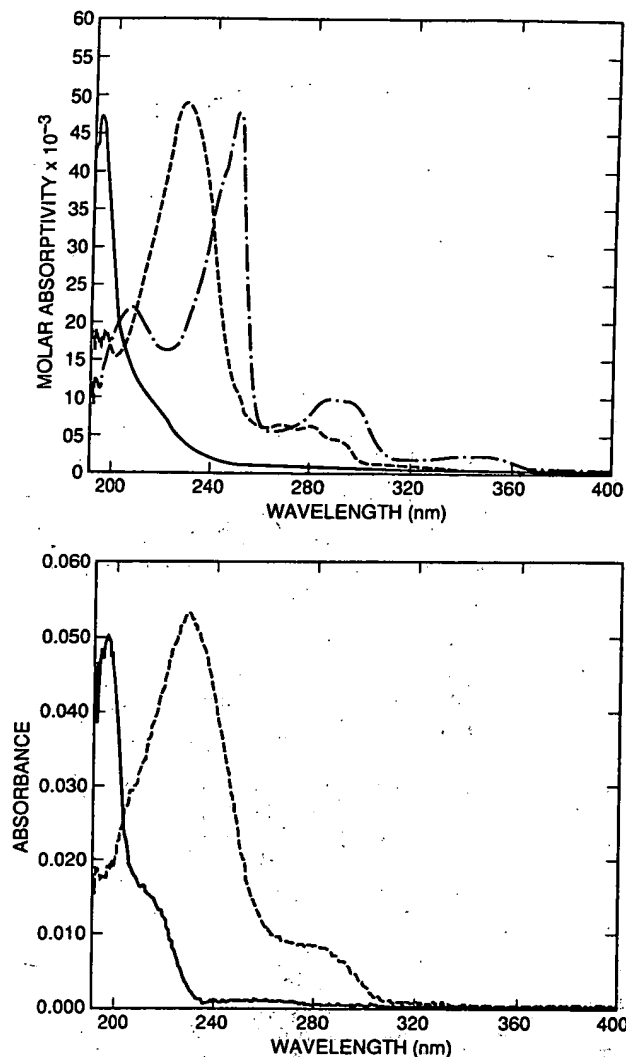


Figure 3. (a, top) Absorbance spectra of PEDA (solid line), NAP-PEDA (dashed line) and NAP-Cl (dot-dashed line) solutions (20 μ M) in acetonitrile. (b, bottom) The absorbance spectra of PEDA (solid line) and NAP-PEDA (dashed line) films on fused silica. Films were prepared as described in Materials and Methods.

lated to a higher dielectric constant within the film.^{21,29} However, the red-shifts are significantly less than those observed for chromophores in Langmuir-Blodgett films²⁹ and well-ordered SAMs.²¹

PEDA films of varying surface coverage were prepared by varying the silanization times between 3 min and 24 h, the reaction temperature between 25 and 100 °C, and the silane concentration between 3.4 and 340 mM PEDAs. The absolute UV absorbance at 195 nm of these films was measured prior to reaction with NAP-Cl. After reaction with NAP-Cl the UV absorbance of each slide was remeasured, the NAP-PEDA difference spectrum was derived, and the NAP-PEDA absorbance at 227.5 nm was determined from the difference spectra. Figure 4 shows the NAP-PEDA absorbance of each film plotted against the corresponding absorbance of the PEDAs prior to the NAP-Cl reaction. This scatter plot shows a nearly monotonic increase in the absorbance of NAP-PEDA formed for a given increase in PEDAs absorbance. PEDAs SAMs with 195.0-nm absorbances greater than 0.09 au could not be formed under the reaction conditions described above. When fused silica slides and native silicon wafers were silanated under the same conditions, fused

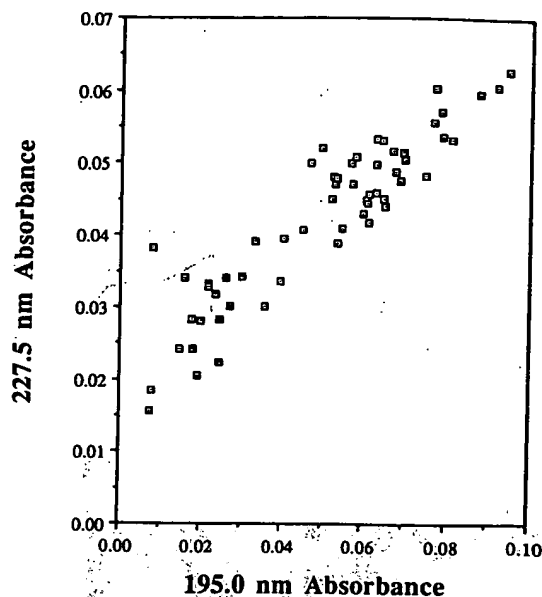


Figure 4. Dependence of NAP-PEDA absorbance on PEDAs absorbance. NAP-PEDA absorbance at 227.5 nm was derived from the difference spectrum of a slide after NAP-Cl reaction minus that of the unmodified PEDAs slide.

silica slides having 195.0-nm absorbance values of between 0.07 and 0.09 au correlated with mean SAM thicknesses of 12 ± 2 Å, as measured by ellipsometry. Thus, PEDAs SAMs greater than one monolayer could not be formed. The advancing water contact angles for these SAMs were in the range of 52–55°.

In order to ascertain possible orientation effects of the NAP-PEDA molecules, the 227.5 nm to 280 nm ratios were calculated for all NAP-PEDA films. The average absorbance for all samples was found to be (0.050 au/0.007 au) with a built in machine noise of 0.001 au, giving a mean ratio of 7.1 with an uncertainty range of 6.25–8.33. No significant changes (i.e., beyond the uncertainty range) in the ratios were observed between solution and surface samples or between surface samples with increasing 227.5-nm absorbance.

Discussion

Changes in the values of λ_{max} and ϵ_{molar} can occur in surface-immobilized chromophores for several reasons: (1) dielectric environment changes,¹¹ (2) ordered packing of the molecules in the monolayer resulting in polarization anisotropy,^{21,30} and/or (3) collective behavior resulting in the formation of new electronic states, as in Davydov splitting.^{14,15} As described above, the optical properties of the PEDAs and NAP-PEDAs in chemisorbed SAMs and in acetonitrile solutions are not significantly different, at least within the noise level inherent with monolayer sample preparations. In addition, the AFM results show that both SAM films are rough and spatially disordered. Both results are consistent with the absence of any collective behavior inducing anisotropic effects or "excimer complexes" in PEDAs and NAP-PEDAs SAMs. This is in contrast to chromophore behavior in well-ordered systems; Langmuir-Blodgett films of anthrylheptanoic acid or cyanine dyes, where intermolecular anisotropic packing results in linear polarization in the optical spectrum and splitting of the wavelength maximum into two longer wavelength peaks^{14,15} and SAMs formed from (11-(2-naphthyl)undecyl)trichlorosilane and octadecyltrichlorosilane, which exhibit large

changes in the absorbance ratio of peaks corresponding to the $^1A \rightarrow ^1B_u$ and $^1A \rightarrow ^1L_a$ transitions of naphthalene.²¹

The above evidence invites hypothetical first-order calculations of molecular packing densities using the operational assumption that the molar extinction coefficients (ϵ_{molar}) of PEDA and NAP-PEDA SAMs are the same as those observed in acetonitrile solution. For solution absorbance, the Beer-Lambert law can be written as follows

$$A = \epsilon_{\text{molar}} bc \quad (2)$$

where ϵ_{molar} is the molar absorptivity coefficient, c is the molar concentration, and b is the path length through the material in question.²⁵ The measured ϵ_{molar} of PEDA is 47 000 M⁻¹ cm⁻¹ at 193 nm and 53 800 M⁻¹ cm⁻¹ for PEDA-NAP at 226.5 nm. To apply eq 2 to the SAMs, the units must be converted to moles and area (cm²). Converting liters to 1000 cm³ gives $\epsilon_{\text{molar}} = 4.73 \times 10^7$ cm² mol⁻¹ for PEDA and $\epsilon_{\text{molar}} = 5.38 \times 10^7$ cm² mol⁻¹ for PEDA-NAP. The term bc is equivalent to s , the molar surface density of a single SAM given in units of mol/cm². Therefore, the relevant equation for the monolayer becomes

$$A = \epsilon_{\text{molar}} s \quad (3)$$

Since both sides of the fused silica slides are silanized, the absorption will be $A = 2\epsilon_{\text{molar}} s$, which when solved for s gives: $s = A/(2\epsilon_{\text{molar}})$.

PEDA SAMs exhibited an upper range of 195-nm absorbances of 0.070–0.090 au. Applying eq 3 to the PEDA SAM, with $\epsilon_{\text{molar}} = 4.73 \times 10^7$ cm² mol⁻¹, results in the calculation of corresponding areas in the range of 17.5–22.5 Å² per PEDA molecule. This range of packing densities corresponds favorably with the estimated density of surface silanols,³¹ and molecular areas observed in LB monolayers of long-chain alcohols¹⁴ (≈ 20 Å²/molecule). The maximum absorbance observed for the various NAP SAM difference spectra was 0.064 au at 227.5 nm. Using the ϵ_{molar} for the NAP-PEDA and substituting into eq 3 yields a corresponding minimum area per NAP-PEDA of 27.9 Å². One should be aware that this value corresponds to the density of reacted NAP on the surface since we are using the difference absorbance at 227.5 nm. One should also be careful not to compare these values to those observed in well-ordered systems, as the values calculated for PEDA and NAP-PEDA films must be considered as spatially and structurally averaged. Nonetheless, these packing densities compare favorably with the range of 21.8–25.2 Å² per molecule previously reported in studies of aromatic trichlorosilane SAMs by X-ray diffraction²³ or LB monolayers composed of aromatic molecules.³²

Since PEDA has two amine groups, NAP-Cl could theoretically react with PEDA in a 2:1 stoichiometry. Thus, the molar ratio of NAP-PEDA to PEDA on a slide reflects the number of amines per PEDA that react with NAP-Cl. The molar ratio can be determined from a surface density measurement of corresponding films of PEDA and NAP-PEDA. The effect of PEDA packing density on amine reactivity is illustrated in Figure 5. At very low calculated PEDA packing densities of (i.e., ~ 1 PEDA per 200 Å²), a nearly complete reaction of PEDA amines and NAP-Cl is observed, yielding 2 NAPs per PEDA. As the SAM packing density increases, however, NAP-PEDA formation per PEDA amine group is dramatically reduced, showing that at the maximum PEDA density of $\sim 10 \times 10^{-10}$ mol/cm², only 60% of the PEDA molecules were successfully reacted with NAP-Cl. It is important to note

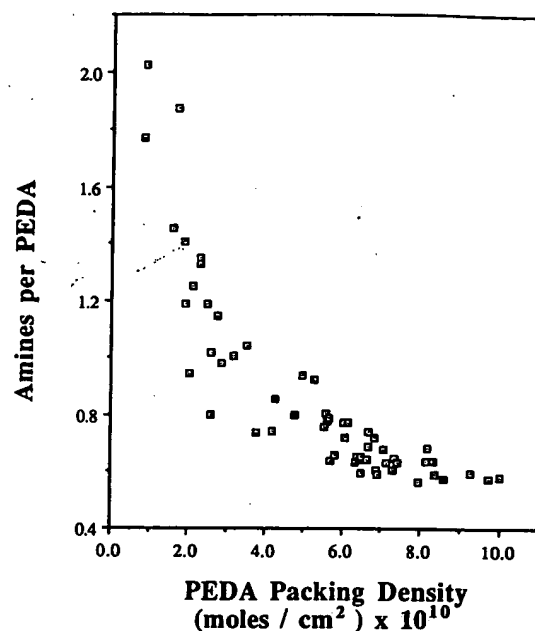


Figure 5. Dependence of PEDA amine reactivity on the calculated PEDA packing density. Moles of NAP-PEDA or PEDA per unit area (cm²) were calculated based on film absorbance as described in the text. The reactivity of amines per PEDA was determined from the quotient of NAP-PEDA surface density and PEDA surface density on each slide.

that the calculated minimum area per NAP-PEDA at this point (27.9 Å²) is only slightly higher than that estimated for naphthalene (25 Å²) in crystal faces,²¹ suggesting that the degree of reaction between PEDA and NAP-Cl is dictated by the maximum possible packing density of the NAP chromophore.

Overall, the results in this paper suggest that PEDA and NAP-PEDA monolayers do not possess the type of order that is commonly associated with deposited LB films or SAMs formed from long-chain organothiols, carboxylic acids, or trichlorosilanes. To our knowledge, this is the first example of using the AFM to distinguish ordered versus disordered packing of self-assembled silane monolayers. One result apparently attributable to this disorder is that constituent chromophores can have UV absorbance spectra that highly resemble the spectra observed in solution. Additional experimental and theoretical work is necessary to establish that solution-derived ϵ_{molar} values for chromophores are useful for an absolute quantitation of their surface packing densities. However, the work presented here shows that a first-order approximation in the present system yields unexpectedly plausible analyses of the quantity of silane molecules deposited per unit area and the role of packing density in defining SAM reactivity.

Acknowledgment. This work was supported in part by the Office of Naval Research and the MANTECH office of the Assistant Secretary of the Navy. D.C.T. and B.M.P. were supported by National Research Council postdoctoral fellowships. We acknowledge the assistance of M.-S. Chen for assistance in film preparations. D.C.T. thanks Dr. Susan Brandow for providing the image of 13F. We acknowledge Dr. Charles Dulcey for the UV acquisition and analysis software, Professors Edward I. Solomon and Curtis Frank (Stanford University) and Dr. J. Hickman (Science Applications International Corporation) for helpful discussions, and the manuscript reviewers for helpful critiques. The opinions and assertions contained herein are the private ones of the authors and are not to be construed as official or reflecting the views of the Department of the Navy.

(31) F6ti, G.; Kov6ts, E. *Langmuir* 1989, 5, 232–239.

(32) Gaines, G. L., Jr. *Insoluble Monolayers at Liquid-Gas Interfaces*; Interscience: New York, 1966.